

## Orphan Spins in the $S = \frac{5}{2}$ Antiferromagnet $\text{CaFe}_2\text{O}_4$

C. Stock,<sup>1</sup> E. E. Rodriguez,<sup>2</sup> N. Lee,<sup>3</sup> F. Demmel,<sup>4</sup> P. Fouquet,<sup>5</sup> M. Laver,<sup>12</sup> Ch. Niedermayer,<sup>6</sup> Y. Su,<sup>7</sup> K. Nemkovski,<sup>7</sup> M. A. Green,<sup>8</sup> J. A. Rodriguez-Rivera,<sup>9,10</sup> J. W. Kim,<sup>3</sup> L. Zhang,<sup>11</sup> and S.-W. Cheong<sup>3</sup>

<sup>1</sup>*School of Physics and Astronomy and Centre for Science at Extreme Conditions, University of Edinburgh, Edinburgh EH9 3FD, United Kingdom*

<sup>2</sup>*Department of Chemistry and Biochemistry, University of Maryland, College Park, Maryland 20742, USA*

<sup>3</sup>*Rutgers Center for Emergent Materials and Department of Physics and Astronomy, Rutgers University, 136 Frelinghuysen Road, Piscataway, New Jersey 08854, USA*

<sup>4</sup>*ISIS Facility, Rutherford Appleton Labs, Chilton, Didcot OX11 0QX, United Kingdom*

<sup>5</sup>*Institute Laue-Langevin, 6 rue Jules Horowitz, Boite Postale 156, 38042 Grenoble Cedex 9, France*

<sup>6</sup>*Laboratory for Neutron Scattering, Paul Scherrer Institut, CH-5232 Villigen, Switzerland*

<sup>7</sup>*Jülich Centre for Neutron Science JCNS, Forschungszentrum Jülich GmbH, Outstation at MLZ, Lichtenbergstraße 1, D-85747 Garching, Germany*

<sup>8</sup>*School of Physical Sciences, University of Kent, Canterbury CT2 7NH, United Kingdom*

<sup>9</sup>*NIST Center for Neutron Research, National Institute of Standards and Technology, 100 Bureau Drive, Gaithersburg, Maryland 20899, USA*

<sup>10</sup>*Department of Materials Science, University of Maryland, College Park, Maryland 20742, USA*

<sup>11</sup>*Laboratory for Pohang Emergent Materials and Max Plank POSTECH Center for Complex Phase Materials, Pohang University of Science and Technology, Pohang 790-784, Korea*

<sup>12</sup>*School of Metallurgy and Materials, University of Birmingham, B15 2TT, United Kingdom*

(Received 12 May 2017; revised manuscript received 4 October 2017; published 22 December 2017)

$\text{CaFe}_2\text{O}_4$  is an anisotropic  $S = \frac{5}{2}$  antiferromagnet with two competing  $A$  ( $\uparrow\uparrow\downarrow\downarrow$ ) and  $B$  ( $\uparrow\downarrow\uparrow\downarrow$ ) magnetic order parameters separated by static antiphase boundaries at low temperatures. Neutron diffraction and bulk susceptibility measurements, show that the spins near these boundaries are weakly correlated and carry an uncompensated ferromagnetic moment that can be tuned with a magnetic field. Spectroscopic measurements find these spins are bound with excitation energies less than the bulk magnetic spin waves and resemble the spectra from isolated spin clusters. Localized bound orphaned spins separate the two competing magnetic order parameters in  $\text{CaFe}_2\text{O}_4$ .

DOI: 10.1103/PhysRevLett.119.257204

Coupling different order parameters often results in new states near the boundary separating them [1–3]. This has been exploited in a variety of fields to engineer unusual properties including in the area of photonics [4,5]. An example also occurs in the vortex state of superconductors where vortices host bound electronic states that differ from the bulk parent metal [6–9]. Fermionic states that exist near boundaries can also be topologically protected [10] resulting in low-energy modes that are robust owing to a symmetry of the underlying Hamiltonian. Examples of such states occur near solitons in polyacetylene [11–14]. However, analogous boundaries and states in magnets, particularly antiferromagnets, have been difficult to identify owing to the absence of a net magnetization, fast dynamics, and the different statistics obeyed by bosonic magnons [15–23]. Here we investigate edge states in the classical and anisotropic antiferromagnetic  $\text{CaFe}_2\text{O}_4$  near the boundary between two competing magnetic order parameters.

$\text{CaFe}_2\text{O}_4$  is a  $S = \frac{5}{2}$  antiferromagnet with an orthorhombic space group (#62  $Pnma$ ,  $a = 9.230$  Å,  $b = 3.017$  Å,  $c = 10.689$  Å) [24–28]. The magnetic structure consists of two competing spin arrangements, termed the  $A$  and  $B$

phases [denoted as ( $\uparrow\uparrow\downarrow\downarrow$ ) ( $\uparrow\downarrow\uparrow\downarrow$ ), respectively], which are distinguished by their  $c$  axis stacking of ferromagnetic  $b$  axis stripes [29]. Neutron inelastic scattering has found that the magnetic exchange coupling in  $\text{CaFe}_2\text{O}_4$  is predominantly two dimensional with strong coupling along  $a$  and  $b$  compared to that along  $c$ . Neutron diffraction has found that the two  $A$  ( $\uparrow\uparrow\downarrow\downarrow$ ) and  $B$  ( $\uparrow\downarrow\uparrow\downarrow$ ) magnetic phases both exist at low temperatures in single crystals and are separated by antiphase boundaries that are confining and result in a countable hierarchy of discrete magnetic excitations [30].

The  $A$  ( $\uparrow\uparrow\downarrow\downarrow$ ) and  $B$  ( $\uparrow\downarrow\uparrow\downarrow$ ) magnetic structures are illustrated in Figs. 1(a) and 1(b), with the magnetic moments aligned along the  $b$  axis (antiparallel arrangements denoted as red and blue). Two possible antiphase boundaries along the  $c$  axis are also illustrated. In Fig. 1(a), the boundary separates two high temperature  $B$  ( $\uparrow\downarrow\uparrow\downarrow$ ) phase structures and locally has the magnetic structure of the low temperature  $A$  phase ( $\uparrow\uparrow\downarrow\downarrow$ ) and also carries a net ferromagnetic moment. A similar situation is presented in Fig. 1(b) for the low temperature  $A$  phase. The momentum broadened rod of diffuse scattering characterizing these boundaries is reproduced in Fig. 1(c) [30].

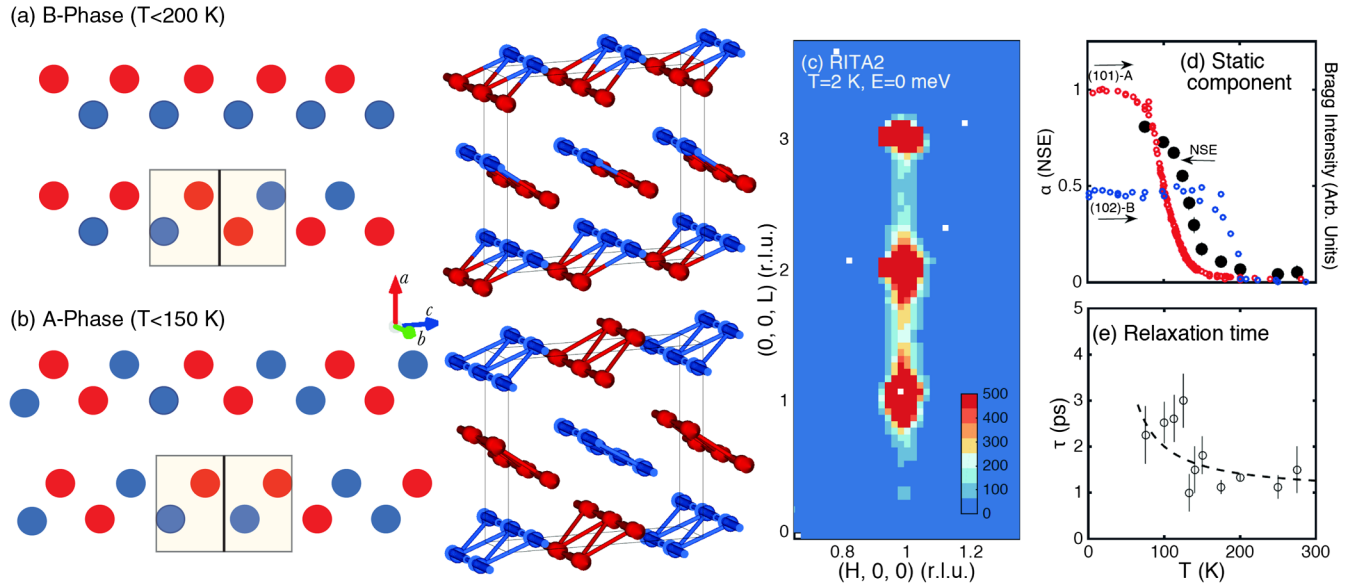


FIG. 1. (a) Illustrates the magnetic  $B$  phase ( $\uparrow\downarrow\uparrow\downarrow$ ) of  $\text{CaFe}_2\text{O}_4$  showing an antiphase boundary where locally (within the highlighted box) the magnetic structure is the  $A$  phase ( $\uparrow\uparrow\downarrow\downarrow$ ). Note that this antiphase boundary carries a net ferromagnetic moment. (b) the same is illustrated for the low temperature  $A$  phase where locally the magnetic structure is the  $B$  phase. (c) illustrates the diffuse scattering cross section characterizing antiphase boundaries. (d–e) show results of a spin echo analysis plotting the fraction of static (on the  $\sim\text{GHz}$  time scale) boundaries and the decay time. The magnetic order parameters of the  $A$  and  $B$  phases extracted from neutron diffraction are also plotted. The dashed line is discussed in the main text.

High resolution neutron spectroscopy [Fig. 1(d) which plots the static fraction  $\alpha$  as a function of temperature] finds these boundaries are predominately static on the GHz time scale below  $\sim 100$  K. The freezing of the boundaries occurs below the onset of  $B$  phase ( $\uparrow\downarrow\uparrow\downarrow$ ) order measured by the (102) magnetic Bragg peak and also higher than the onset of  $A$  phase ( $\uparrow\uparrow\downarrow\downarrow$ ) order probed through measurements of (101). The relaxational time scale measured with spin echo is displayed in Fig. 1(e), where the dashed line is a plot of  $\tau = \exp(U/k_B T)$  with  $U$  fixed at the bulk magnetic anisotropy gap of 5 meV measured with neutron spectroscopy [30]. The data are consistent with antiphase boundaries relaxing with an energy fixed by the bulk spin anisotropy.

The presence of static boundaries separating  $A$  and  $B$  order parameters brings the possibility of magnetic states that have different properties from the bulk, termed orphan spins [31–33]. We apply neutron diffraction and inelastic scattering to identify and characterize these states. Further experimental details are provided in the Supplemental Material [34].

We first investigate the static structure of the antiphase boundaries using the DNS polarized diffractometer applying an  $XYZ$  polarization geometry. Figure 2 illustrates the background corrected magnetic scattering originating from  $\text{Fe}^{3+}$  moments pointing along  $Y$  and  $Z$  (with  $Z$  vertical and parallel to the crystallographic  $b$  axis and  $Y$  in the horizontal ( $HOL$ ) scattering plane and perpendicular to  $\vec{Q}$ ). Figures 2(a)–(d) plot the magnetic intensity at 100 K and 50 K displaying two components—momentum resolution limited Bragg peaks at the integral  $(H, 0, L)$  positions,

corresponding to the long-range bulk structure, and a component which is broadened along the  $(1, 0, L)$  direction originating from short range spin correlations associated with the antiphase boundaries. The intensity contours illustrate that while most of the low-temperature magnetic scattering originates from spins aligned parallel to the  $b$  axis ( $Z$  direction), there is a measurable momentum broadened fraction of the intensity originating from moments perpendicular to this direction along  $Y$ . Figure 2(e) plots the temperature evolution of the two components divided by the total magnetic intensity from the  $X$  direction showing a significant fraction of spins jam perpendicular to the crystallographic  $b$ -axis while the  $\text{Fe}^{3+}$  moments reorient from  $B$  ( $\uparrow\downarrow\uparrow\downarrow$ ) phase to  $A$  ( $\uparrow\uparrow\downarrow\downarrow$ ) phase order on cooling. The polarized results illustrate that there is a gradual change in the spin direction across the domain wall reminiscent of a “Bloch” wall instead of a fully discontinuous  $180^\circ$  “Neel” type boundary.

We now investigate whether these boundaries are tunable with an applied magnetic field [35]. Magnetization loops at 120 K and 5 K in Fig. 3(a) find an uncompensated remanent moment when the field is applied along  $b$ . Panels 3(b),(c) illustrated the temperature and magnetic field dependence of the elastic diffuse scattering (RITA2 with unpolarized neutrons) at  $\vec{Q} = (-1, 0, 1.4)$  and  $(-1, 0, 1.65)$  under different applied field conditions and representative ( $HOL$ ) maps are displayed in panels 3(d)–(f). The peak in intensity at  $\sim 200$  K [panels 3(b),(c)] is associated with critical scattering of the high temperature  $B$  phase ordering [panels 3(d)–(f)]. A minimum in the temperature dependent intensity [panels 3(b),(c)] is seen at  $\sim 150$  K before rod like

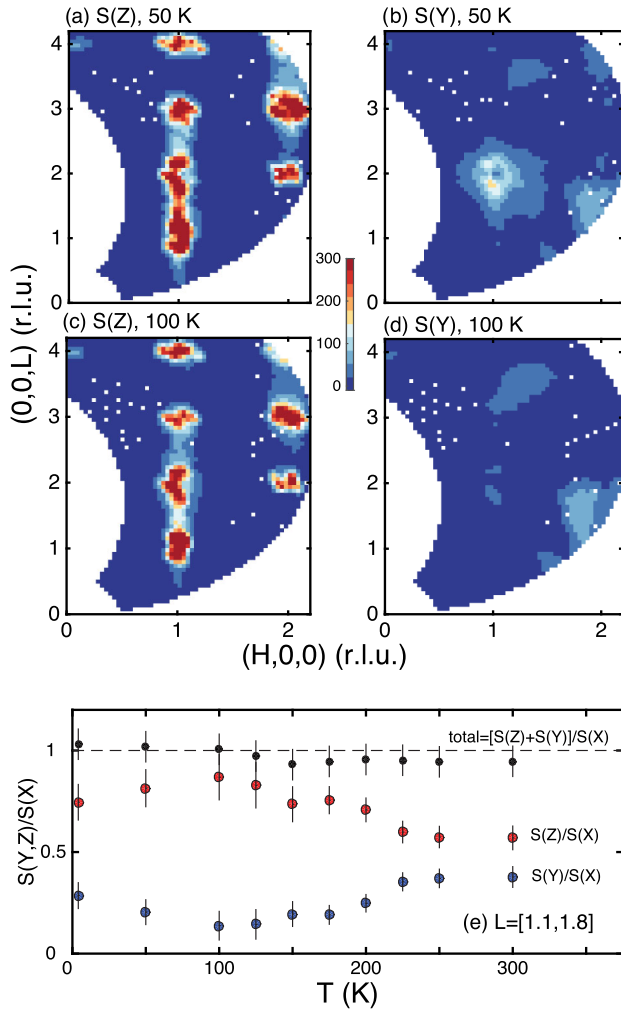


FIG. 2. Polarized (magnetic) diffuse scattering where  $X$  is parallel to  $\vec{Q}$ ,  $Y$  perpendicular and within the  $(HOL)$  plane, and  $Z$  along  $b$ . Panels (a) and (c) show the magnetic scattering originating from spins aligned along the crystallographic  $b$  axis at 100 and 50 K. (b) and (d) show the same but for the spins oriented perpendicular to  $b$ . (e) plots the fraction of intensity originating from spins aligned along  $Y$  and  $Z$ . The total is shown to be in agreement of 1, required from sum rules for polarized neutron scattering.

scattering along  $L$  characteristic of static antiphase boundaries forms [panel 3(d) at 75 K]. Panels 3(b),(c) show that the intensity is hysteretic in temperature with a peak forming at  $\sim 100$  K on warming analogous to localized structures in disordered materials (for example ferroelectric  $K_{1-x}Li_xTaO_3$  [36]).

Figures 3(b) and 3(c) also display the temperature dependence of this diffuse scattering cross section in the case of differing field conditions. When cooling takes place in an 11 T field parallel to the  $b$  axis [panel (b)], the diffuse scattering is enhanced in comparison to the zero field cooled (ZFC) temperature sweep. No field dependence in this enhancement was observed for  $\mu_0 H$  greater than 1 T and the effect was observed to freeze in for cooling below

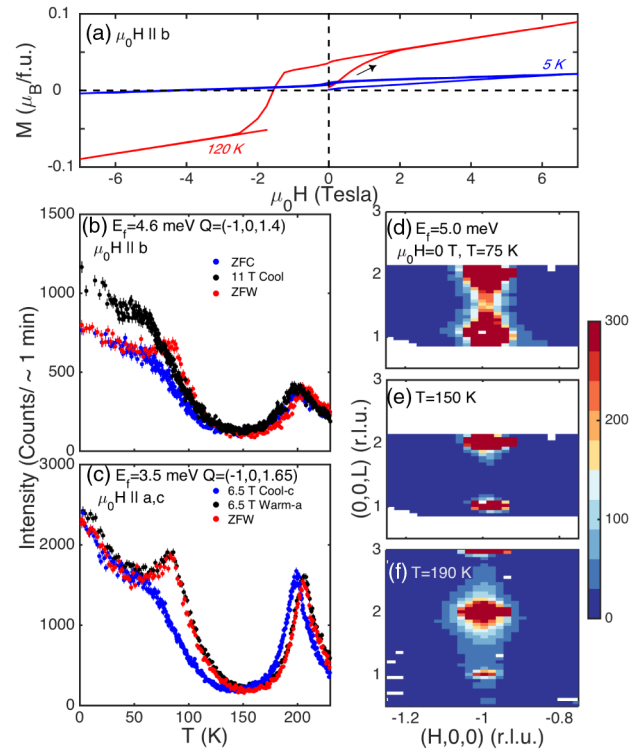


FIG. 3. (a) Magnetization loops at 120 K and 5 K illustrating a remanent magnetization in  $CaFe_2O_4$ . (b) plots the temperature dependence at  $\vec{Q} = (-1, 0, 1.4)$ . Zero field cooled (ZFC), zero field warmed (ZFW), and 11 T field cooled data were taken with the field  $\parallel b$  (vertical) axis. (c) illustrates the same cooling sequences at  $\vec{Q} = (-1, 0, 1.65)$  with the field aligned perpendicular to the  $b$  axis and in the  $(HOL)$  scattering plane. (d–f) plots the diffuse scattering cross section in zero field at 75 K, 150 K, and 190 K. Further details on the experimental configuration and zero field susceptibility are given in the Supplemental Material [34].

$\sim 150$  K. Panel (c) illustrates that this enhancement is largely reduced when the field is perpendicular to the  $b$  axis as shown using a horizontal magnetic field of 6.5 T. The comparatively small changes with the field perpendicular to the  $b$  axis is consistent with the relatively small number of spins jammed perpendicular to  $b$  discussed above in the context of Fig. 2. Due to kinematic constraints associated with the horizontal magnet, an  $E_f = 3.5$  meV was used providing different intensity ratios for the diffuse scattering measured at  $\sim 200$  K in comparison to base temperature owing to differing energy resolutions and spectrometer configurations. Therefore, cooling with the field aligned along the direction of dominant bulk staggered magnetization (crystallographic  $b$  axis) results in an enhancement of diffuse scattering indicative of a larger density of antiphase boundaries. Orienting the field perpendicularly does not result in any such enhancement.

The response of the diffuse scattering to an applied magnetic field that tracks the dominant orientation indicates that these boundaries have a  $b$  axis uncompensated,

ferromagnetic moment. While this conclusion is drawn from the finite- $Q$  response, magnetization [panel (a),  $Q = 0$  probe] corroborates the presence of a localized ferromagnetic moment and further data presented in the Supplemental Material [34] show the momentum dependence is indeed peaked at  $Q = 0$ . One such real-space scenario for this to occur is illustrated in Fig. 1(a) which schematically plots an antiphase boundary in the high temperature  $B$  phase. Locally, the orphaned spins in the boundary have the structure of the low temperature  $A$  phase and also carry a net ferromagnetic moment which originates in the field dependence presented in Fig. 3. This local ferromagnetism occurs even though the magnetic structure is globally antiferromagnetic.

We now apply spectroscopy to study the energy spectra associated with these antiphase boundaries. Magnetic boundary, or edge, states have been predicted in low dimensional magnets [37] and superconductors [38] and experimentally observed in insulating and disordered quantum magnets [39–43]. Motivated by the possibility of novel states near these boundaries, we apply neutron spectroscopy in Fig. 4 by searching for bound magnetic excitations within the anisotropy induced gap of  $\sim 5$  meV. Figure 4(a) illustrates a constant momentum scan (RITA2) showing a peak at 0.9 meV. The peak is significantly broader than resolution (solid horizontal line of 0.25 meV) with a full width in energy of  $2\Gamma = 0.72 \pm 0.15$  meV and approximately an order of magnitude weaker in intensity than the bulk dispersive spins waves. Panel (b) plots a constant energy slice indicating strong correlations along the  $a$  axis and weak correlations along  $c$  mimicking the elastic magnetic diffuse scattering cross section [Fig. 1(c)]. Figure 4 panel (c) shows an energy slice using high resolution neutron spectroscopy from the OSIRIS backscattering spectrometer. The mode at 0.9 meV, while broader than resolution, displays no momentum dispersion and hence no on site molecular field, indicative of isolated or orphan spins states.

The energy scale of 0.9 meV can be reconciled if we consider a simple edge state consisting of isolated clusters. Such clusters consist of  $S = \frac{5}{2}$   $\text{Fe}^{3+}$  spins coupled with an exchange constant along the crystallographic  $c$  axis with an interaction Hamiltonian of  $H = J_c \sum_{ij} \vec{S}_i \cdot \vec{S}_j$  (where  $i, j$  is summed over the cluster) [44,45]. The simplest state would consist of an isolated dimer with a singlet  $j_{\text{eff}} = 0$  ground state and higher energy levels of  $j_{\text{eff}} = 1, 2, 3, 4, 5$ . The energy scale to excite such a dimer from the ground state to an excited state is  $= J_c$  which has been estimated to be  $0.94 \pm 0.19$  meV based on high energy spectroscopy of the bulk magnetic dispersion discussed previously [30]. This is in agreement with the peak position in Fig. 4(a). However, Fig. 4(c) also displays a continuum of excitations that extend from  $E = 0.9$  meV to higher energies that can be understood in terms of larger clusters, such as trimers, which would display discrete excitations at further energies. The energy spectrum for the above Hamiltonian based

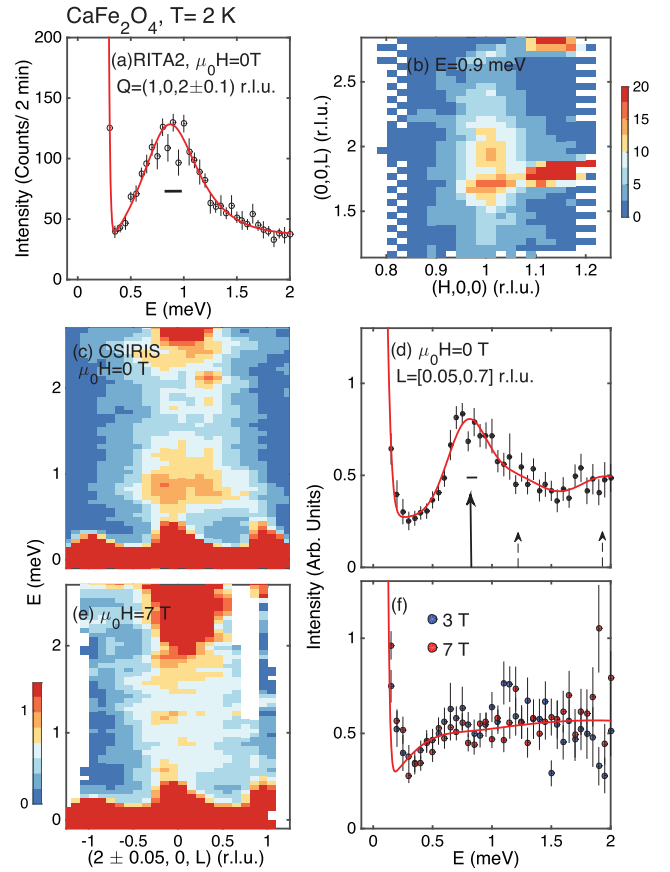


FIG. 4. (a) displays a constant- $Q$  scan showing the presence of an in-gap mode at low temperatures fit to a harmonic oscillator line shape. (b) illustrates a constant energy slice showing that the intensity is elongated along  $L$ . (c–f) displays high resolution scans taken on OSIRIS showing the gapped excitation and the response to 3T and 7T applied along the crystallographic  $b$  axis. The solid line in (d) is a fit to underdamped harmonic oscillators with positions fixed to be the calculated dimer (solid arrow) and trimer (dashed arrows) positions. The fit in (f) is to a single damped harmonic oscillator.

on a trimer would display its lowest excitation energies of  $1.5J_c$ ,  $2.5J_c$ , and  $3.5J_c$ . [46] The solid line in panel 4(d) is a fit to the OSIRIS data to a series of lifetime shortened excitations fixed at the dimer excitation level and the two lowest energy trimer levels with the intensity reflecting the probability of such states. From this fit to dimer and trimers, we get an estimate of  $J_c = 0.78 \pm 0.17$  meV, which is in agreement with the value obtained from fitting the dispersive band excitations.

Figures 4(e) and 4(f) illustrate the response of these cluster states to an applied magnetic field, showing that applied fields of 3T and 7T along the crystallographic  $b$  axis are sufficient to smear the lowest energy state in energy. These results are consistent with Zeeman splitting of lifetime shortened multiplets originating from cluster excitations. The fit in panel 4(f) is to a single energy broadened relaxational mode. The results of this analysis

shows that the exchange constant derived from the higher energy bulk spin wave measurements and the localized excitations from the “in-gap” states can be consistently understood by the presence of clusters of spins located near the antiphase boundaries. The energy scale of these cluster states is low enough to be tuned with a field.

The magnetic bound states display weak dynamic correlation lengths along  $c$ , while much longer length scales exist along  $a$ , therefore mimicking the planar antiphase boundaries found in diffraction and differing from the spin waves onset at much higher energies. The lack of a measurable on site molecular field evidenced from the momentum dependence indicates that these orphaned spins are decoupled from the  $A$  and  $B$  magnetic order parameters. These orphaned states exist at the boundary between the two order parameters allowing them to coexist in  $\text{CaFe}_2\text{O}_4$  at low temperatures. Such states have been proposed as a means of stabilizing spin liquid states in honeycomb lattices [47] and may exist in triangular magnets with much smaller exchange interactions resulting in strong low-energy fluctuations [48–50]. Orphaned spins may be a means of decoupling differing magnetic orders when a number of different order parameters exist with similar energy scales.

In summary, we have shown the presence of ferromagnetic edge states in  $\text{CaFe}_2\text{O}_4$  originating from antiphase boundaries separating competing magnetic order parameters. Spectroscopic evidence points to these edge states consisting of clusters of orphaned spins.

This work was supported by the EPSRC, the Carnegie Trust for the Universities of Scotland, the Royal Society of London, and Royal Society of Edinburgh, the STFC, EU-NMI3, NSF (No. DMR-1508249), and the Swiss spallation neutron source (SINQ) (Paul Scherrer Institute, Villigen, Switzerland). The work at Rutgers was supported by the DOE under Grant No. DE-FG02-07ER46382. The work at Postech was supported by the Max Planck POSTECH/KOREA Research Initiative Program [Grant No. 2011-0031558] through NRF of Korea funded by MSIP. We thank C. Mudry (PSI) for helpful discussions.

---

[1] W. Shockley, *Phys. Rev.* **56**, 317 (1939).  
 [2] D. L. Mills and W. M. Saslow, *Phys. Rev.* **171**, 488 (1968).  
 [3] D. L. Mills, *Phys. Rev. Lett.* **20**, 18 (1968).  
 [4] J. Li, L. Zhou, C. T. Chan, and P. Sheng, *Phys. Rev. Lett.* **90**, 083901 (2003).  
 [5] S. Enoch, G. Tayeb, P. Sabouroux, N. Guérin, and P. Vincent, *Phys. Rev. Lett.* **89**, 213902 (2002).  
 [6] A. W. Overhauser and L. L. Daemen, *Phys. Rev. Lett.* **62**, 1691 (1989).  
 [7] H. F. Hess, R. B. Robinson, R. C. Dynes, J. M. Valles, and J. V. Waszczak, *Phys. Rev. Lett.* **62**, 214 (1989).  
 [8] N. Hayashi, T. Isoshima, M. Ichioka, and K. Machida, *Phys. Rev. Lett.* **80**, 2921 (1998).

[9] S. H. Pan, E. W. Hudson, A. K. Gupta, K.-W. Ng, H. Eisaki, S. Uchida, and J. C. Davis, *Phys. Rev. Lett.* **85**, 1536 (2000).  
 [10] M. Z. Hasan and C. L. Kane, *Rev. Mod. Phys.* **82**, 3045 (2010).  
 [11] S. P. Su and J. R. Schrieffer, *Proc. Natl. Acad. Sci. U.S.A.* **77**, 5626 (1980).  
 [12] A. J. Heeger, S. Kivelson, J. R. Schrieffer, and W. P. Su, *Rev. Mod. Phys.* **60**, 781 (1988).  
 [13] S. Roth and H. Bleier, *Adv. Phys.* **36**, 385 (1987).  
 [14] L. Rothberg, T. M. Jedju, S. Etemad, and G. L. Baker, *Phys. Rev. Lett.* **57**, 3229 (1986).  
 [15] A. V. Kimel, A. Kirilyuk, A. Tsvetkov, R. V. Pisarev, and T. Rasing, *Nature (London)* **429**, 850 (2004).  
 [16] T. Jungwirth, X. Marti, P. Wadley, and J. Wunderlich, *Nat. Nanotechnol.* **11**, 231 (2016).  
 [17] T. Shiino, S. H. Oh, P. M. Haney, S. W. Lee, G. Go, B. G. Park, and K. J. Lee, *Phys. Rev. Lett.* **117**, 087203 (2016).  
 [18] O. Gomonay, T. Jungwirth, and J. Sinova, *Phys. Rev. Lett.* **117**, 017202 (2016).  
 [19] T. Kampfrath, A. Sell, G. Klatt, A. Pashkin, S. Mahrlein, T. Dekorsy, M. Wolf, M. Fiebig, A. Leitenstorfer, and R. Huber, *Nat. Photonics* **5**, 31 (2011).  
 [20] M. Bode, E. Y. Vedmedenko, K. von Bergmann, A. Kubetzka, P. Ferriani, S. Heinze, and R. Wiesendanger, *Nat. Mater.* **5**, 477 (2006).  
 [21] W. H. Meiklejohn and C. P. Bean, *Phys. Rev.* **102**, 1413 (1956).  
 [22] W. H. Meiklejohn and C. P. Bean, *Phys. Rev.* **105**, 904 (1957).  
 [23] L. Zhang, J. Ren, J.-S. Wang, and B. Li, *Phys. Rev. B* **87**, 144101 (2013).  
 [24] D. F. Decker and J. S. Kasper, *Acta Crystallogr.* **10**, 332 (1957).  
 [25] P. M. Hill, H. S. Peiser, and J. R. Rait, *Acta Crystallogr.* **9**, 981 (1956).  
 [26] Y. Allain, B. Boucher, P. Imbert, and M. Perrin, *C. R. Acad. Sci. Paris* **263**, 9 (1966).  
 [27] H. Watanabe, H. Yamauchi, M. Ohashi, M. Sugiimoto, and T. Okada, *J. Phys. Soc. Jpn.* **22**, 939 (1967).  
 [28] R. Das, S. Karna, Y. C. Lai, and F. C. Chou, *Cryst. Growth Des.* **16**, 499 (2016).  
 [29] K. Obata, Y. Obukuro, S. Matsushima, H. Nakamura, M. Arai, and K. Kobayashi, *J. Ceram. Soc. Jpn.* **121**, 766 (2013).  
 [30] C. Stock, E. E. Rodriguez, N. Lee, M. A. Green, F. Demmel, R. A. Ewings, P. Fouquet, M. Laver, C. Niedermayer, Y. Su, K. Nemkovski, J. A. Rodriguez-Rivera, and S. W. Cheong, *Phys. Rev. Lett.* **117**, 017201 (2016).  
 [31] R. Moessner and A. J. Berlinsky, *Phys. Rev. Lett.* **83**, 3293 (1999).  
 [32] P. Schiffer and I. Daruka, *Phys. Rev. B* **56**, 13712 (1997).  
 [33] J. Rehn, A. Sen, and R. Moessner, *Phys. Rev. Lett.* **118**, 047201 (2017).  
 [34] See Supplemental Material at <http://link.aps.org/supplemental/10.1103/PhysRevLett.119.257204> for experimental details, sample characterization, and more information regarding excitations in magnetic clusters.  
 [35] N. Papanicolaou, *J. Phys. Condens. Matter* **10**, L131 (1998).  
 [36] C. Stock, P. M. Gehring, G. Xu, D. Lamago, D. Reznik, M. Russina, J. Wen, and L. A. Boatner, *Phys. Rev. B* **90**, 224302 (2014).

- [37] T. K. Ng, *Phys. Rev. B* **50**, 555 (1994).
- [38] H. Kohno, H. Fukuyama, and M. Sigrist, *J. Phys. Soc. Jpn.* **68**, 1500 (1999).
- [39] G. Xu, C. Broholm, Y. A. Soh, G. Aeppli, J. F. DiTusa, Y. Chen, M. Kenzelmann, C. D. Frost, T. Ito, K. Ota, and H. Takagi, *Science* **317**, 1049 (2007).
- [40] M. Kenzelmann, G. Xu, I. A. Zaliznyak, C. Broholm, J. F. DiTusa, G. Aeppli, T. Ito, K. Oka, and H. Takagi, *Phys. Rev. Lett.* **90**, 087202 (2003).
- [41] G. Els, G. S. Uhrig, P. Lemmens, H. Vonberg, P. H. M. van Loosdrecht, G. Guntherodt, O. Fujita, J. Akimitsu, G. Ghalenne, and A. Revcolevschi, *Europhys. Lett.* **43**, 463 (1998).
- [42] D. Schmidiger, K. Y. Povarov, S. Galeski, N. Reynolds, R. Bewley, T. Guidi, J. Ollivier, and A. Zheludev, *Phys. Rev. Lett.* **116**, 257203 (2016).
- [43] C. Stock, W. J. L. Buyers, K. C. Rule, J. H. Chung, R. Liang, D. Bonn, and W. N. Hardy, *Phys. Rev. B* **79**, 184514 (2009).
- [44] W. J. L. Buyers, T. M. Holden, E. C. Svensson, and D. J. Lockwood, *Phys. Rev. B* **30**, 6521 (1984).
- [45] A. Furrer and O. Waldmann, *Rev. Mod. Phys.* **85**, 367 (2013).
- [46] E. C. Svensson, M. Harvey, W. J. L. Buyers, and T. M. Holden, *J. Appl. Phys.* **49**, 2150 (1978).
- [47] R. Flint and P. A. Lee, *Phys. Rev. Lett.* **111**, 217201 (2013).
- [48] E. Lhotel, V. Simonet, J. Ortloff, B. Canals, C. Paulsen, E. Suard, T. Hansen, D. J. Price, P. T. Wood, A. K. Powell, and R. Ballou, *Phys. Rev. Lett.* **107**, 257205 (2011).
- [49] C. Stock, S. Jonas, C. Broholm, S. Nakatsuji, Y. Nambu, K. Onuma, Y. Maeno, and J.-H. Chung, *Phys. Rev. Lett.* **105**, 037402 (2010).
- [50] Y. Nambu, J. S. Gardner, D. E. MacLaughlin, C. Stock, H. Endo, S. Jonas, T. J. Sato, S. Nakatsuji, and C. Broholm, *Phys. Rev. Lett.* **115**, 127202 (2015).